# Dual-band (28/38 GHz) MIMO Antenna System for 5G Mobile Communications with Efficient DoA Estimation Algorithm in Noisy Channels

**Asmaa E. Farahat and Khlaid F. A. Hussein**

Microwave Engineering Department
Electronics Research Institute, Cairo, 11843, Egypt
asmaa@eri.sci.eg, Khalid_elgabaly@yahoo.com

***Abstract*** ─ In this paper, a dual-band (28/38 GHz) linear antenna arrays of four and eight elements are proposed to work as a MIMO arrays for the 5G communication systems. Each element in the array is a dual-band Yagi-Uda antenna designed to operate at 28 and 38 GHz. The eight-elements array size has a total dimension of 79.4 mm × 9.65 mm excluding the feeding microstrip line. The maximum gain of the array is about 18 dB. The peaks of correlation at matched angles (PCMA) technique is applied to determine the direction of arrival for multiple incoming signals. The effects of phase noise and additive Gaussian noise on the error in the DoA estimation are studied showing good accuracy of the PCMA algorithm. Numerical and experimental investigations are achieved to assess the performance of both the single-element antenna and the eight-element MIMO linear antenna array. It is shown that the simulation results agree with the experimental measurements and both show good performance of the single antenna as well as the MIMO linear array system. The envelope correlation coefficient (ECC) and the diversity gain (DG) are calculated and the results show that the proposed MIMO antenna system is suitable for the forthcoming 5G mobile communications. The radiation patterns for single antenna and four-element array are measured and compared to the electromagnetic simulation results showing good agreement.

***Index Terms*** ─ DoA, MIMO array, Yagi-Uda.

## I. INTRODUCTION

Recently, the mm-wave in the 28 GHz and 38 GHz frequency bands has been reported to be used in wireless cellular communication systems [1]. Higher bandwidths for higher data rates are required for the future 5th generation mobile communication. This is provided by the millimeter wave bands [2]. Unfortunately, the wavelength of the signal becomes shorter as the operating frequency increases, and consequently the free-space path loss becomes higher, according to Friis transmission equation [3]-[4]. High gain antennas are needed to compensate for the free-space path losses and various forms of fading that can be observed in the communication channel [5], [6]. When considering multipath effects, the MIMO antenna system can offer many advantages. Good circuit solutions for mobile communication applications at mm-wave frequencies are achieved by using both high gain and MIMO configurations. This reduces the operating costs of any required supporting power amplifiers and control circuitry [7]. The estimated bands under consideration for 5G technology are the frequency spectrum around 28 GHz, 38 GHz, 60 GHz and 73 GHz. These millimeter wave bands would bring new challenges in the MIMO antennas implementation for handheld devices [8].

Dual band MIMO antennas have been reported in literature. A 4 × 4 28/38 dual-band MIMO antenna system with a round patch EBG Cell is introduced in [8]. Also, a dual band MIMO antenna composed of two orthogonal elements operating in the frequency bands 1.62-3.2 GHZ and 4.4-5.9 GHz is introduced in [9]. A dual band 28/45 microstrip circular patch antenna with an elliptical slot is presented in [10], with bandwidths of 1.3 GHz at 28 GHz and 1GHz at 45 GHz.

The DoA estimation is one of the key issues in the discipline of array signal processing and finds applications in the fields of radar, sonar, and wireless positioning applications [11]. The most popular DoA estimation algorithms commonly used are the maximum likelihood (ML) [12], multiple signal classification (MUSIC) [13], and estimation of signal parameters via rotational invariance techniques [14]. The DoA estimation technique used in this work is adapted from the peaks of the correlation at matched angles (PCAMA) technique proposed in [15].

## II. THE PROPOSED YAGI_UDA ANTENNA AND ARRAY STRUCTURE

The present section describes the design of the proposed Yagi-Uda antenna used to construct the MIMO linear array system. Antenna is constructed as a driven dipole antenna, one director and two reflectors. Each reflector has a triangular shape to enhance the antenna gain. The length of the dipole is set to resonate at 38 GHz. Three equally spaced corrugations are added to

*Submitted On: November 15, 2020*
*Accepted On: January 18, 2021*

https://doi.org/10.47037/2020.ACES.J.360308

each dipole arm with dimensions set for good impedance matching. An extension strip is capacitively end-coupled to each dipole arm through an infinitesimal gap for dual-band operation. The total length of the gap and the extension strip are set such that extended corrugated dipole has additional resonance at 28 GHz. The driven dipole is fed through a transmission line of two parallel strips; one f them is printed on the top layer of the substrate and the other is printed on the bottom layer. For practical measurements using coaxial feed line, three stage microstrip line transitions is used between the coaxial feeder and the two-strip line. The transition is composed of three cascaded strip line regions with different lengths and widths designed for 50 Ω impedance matching. One of the dipole arms and its extension are printed on the bottom layer of the substrate and connected to the ground plane. The arrangement of the proposed antenna structure with the dimensional parameters is shown in Fig. 1. The MIMO array of this Yagi-Uda antenna is shown in Fig. 2.

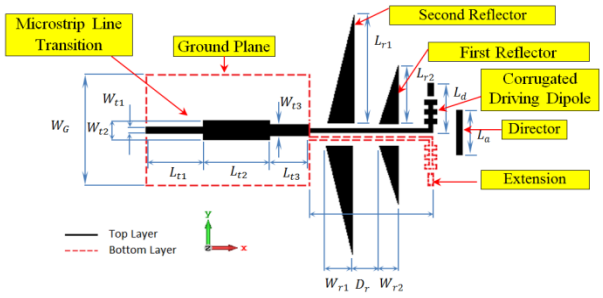


Fig. 1. Dual-band 28/38 GHz Yagi-Uda antenna.

## III. DIRECTION OF ARRIVAL (DOA) ESTIMATION ALGORITHM

The DoA estimation algorithm applied to the proposed MIMO linear array is adapted from the PCMA algorithm presented in [15] for planar arrays. The PCMA is an efficient technique for detecting the DoA that depends on the correlation matrix between the steering matrix of the array and the matrix representing the received signals at the array elements. This correlation matrix will have its main diagonal elements nearly pure real when the steering matrix is set to get the same direction of maximum radiation of the array as the direction of arrival of one of the received signals.

The steering matrix for a linear array of $N$ isotropic point sources can be written in the form:

$$\mathbf{S}(\theta) = [s_n(\theta)]_{n=1,2,..,N} = \left(e^{j\psi_1} \quad e^{j\psi_2} \quad \dots \quad e^{j\psi_N}\right), \tag{1}$$

where $\psi_n$ is the phase of excitation of the $n^{th}$element of the linear array that can be expressed as:

$$\psi_n = (n-1)\beta, \quad n = 1,2,..,N, \tag{2}$$

where $\beta$ is the progressive phase shift of the element excitations which can be expressed as:

$$\beta(\theta) = k_o \Delta sin\theta, \tag{3}$$

where $k_o$ is the free space wave number and $\Delta$ is the spacing between the array elements.

Assuming $p$ incoming waves, let the received voltage due to the $p^{th}$ incoming wave under the effect of noise be,

$$\mathbf{X}_p = \alpha_p \mathbf{S}_p e^{j\varphi_e} + \mathbf{N}(\theta_p), \qquad p = 1,2,\dots,P, \tag{4}$$

where $\alpha_p$ is constant proportional to the strength of the $p^{th}$ arriving signal, $\mathbf{S}_p$ is the steering matrix, $\varphi_e$ is the phase error due to phase noise, and $\mathbf{N}(\theta_p)$ is the additive noise. It is assumed that each $p$ incoming signal has different noise power level.

Consider the following correlation matrix:

$$\mathbf{R}_p(\theta) = E\{\mathbf{S}(\theta)\mathbf{X}_p^H\}, \qquad p = 1,2,\dots,P, \tag{5}$$

where the operator $E\{\cdot\}$ means the expected or mean value of the operand, $\mathbf{S}(\theta)$ is the steering matrix at $\theta$ direction. $H$ is the hermitian operator.

At very high signal to noise ratio (SNR), i.e., $\varphi_e \approx 0$, and $A_p \approx 0$, the main diagonal elements of the matrix $\mathbf{R}_p(\theta)$ are approximately pure real at $\theta = \theta_p$. For an $N$-elements linear array, the $\mathbf{R}_p$ matrix can be written as,

$$\mathbf{R}_p(\theta) = \left[r_{p_{m,n}}(\theta,\phi)\right]_{\substack{m=1,2,\dots,N,\\ n=1,2,\dots,N}} \quad p = 1,2,\dots,P, \tag{6}$$

At low noise to carrier power ratio (NCR) or high SNR, each of the complex quantities $r_{p_{m,n}}(\theta,)$ has its imaginary part tending to zero as the angle $\theta$ approaches $\theta_p$. Thus, the following quantity is important and can be used to detect the directions of arrival of multiple signals:

$$d_p(\theta) = \sum_{n=1}^{N} \frac{|imag(r_{p_{m,n}})|}{|r_{p_{m,n}}|^4}, \quad m = n. \tag{7}$$

Consequently, the peaks of the following function, when plotted against $\theta$ in the half-space domain, $0 < \theta < \frac{\pi}{2}$ give the angles determining the DoA for all the incoming signals,

$$P_{CAMA}(\theta) = \sum_{p=1}^{P} \frac{1}{d_p(\theta)}, \qquad p = 1,2,\dots,P. \tag{8}$$

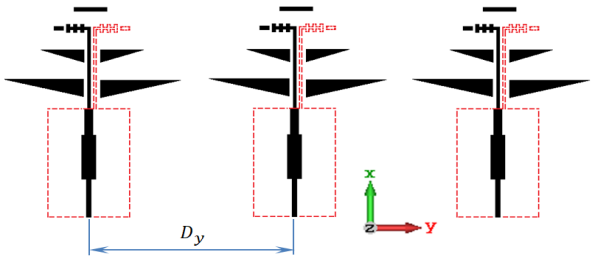


Fig. 2. MIMO array configuration of the proposed Yagi-Uda antenna.

## IV. PHASE NOISE MODEL

Studying the effect of the phase error encountered due to the phase noise is of particular importance as the PCMA technique depends on the correctness and accuracy of the phases of the signals received at the array elements. The phase noise model presented in [16] is used to study the effect of phase noise on the PCMA technique. The phase noise is commonly characterized by its single-side band power spectral density (PSD), $L(f)$, in the frequency domain which is defined as the noise power within a bandwidth of 1 Hz at an offset frequency, $f$, from the carrier frequency relative to the carrier power $P_r$ [16]. Hence, $L(f)$ is expressed as:

$$L(f) = \frac{\text{Noise power in 1Hz bandwidth}}{P_r}. \quad (9a)$$

To study the effect of phase noise on the error in the phase of the incoming signal, it is required to determine the instantaneous phase error samples.

As phase noise causes spectrum broadening, its effect is described by the noise-to-carrier power ratio (NCR) which is the ratio between the power contained within a bandwidth $\Delta f$ around the carrier, and the power of the carrier,

$$\text{NCR} = 2\int_0^{\Delta f/2} L(f)\, df. \quad (9b)$$

Let the signal $s(t)$ received at the port of an antenna element of the array in the time domain be expressed as:

$$s(t) = V_o\, e^{j(2\pi f_r t + \psi_n + \varphi_e(t))}, \quad (10)$$

where $V_o$ is the amplitude of the received signal, $f_r$ is the frequency, $\psi_n$ is the phase due to the path travelled by the signal received at the element number $(n)$ of the linear array, and $\varphi_e(t)$ is the unknown instantaneous value of the phase error due to the phase noise. In the frequency domain, the discrete frequency domain samples $S_k$ of the received signal are constructed as,

$$S_k = S(f_k) = A_k\, e^{j\psi_k}, \qquad k = 1,2,..,K, \quad (11)$$

where the discrete phase samples $\psi_k$ are generated as a sequence of uniformly distributed random numbers in the closed interval $[-\pi, \pi]$ and the discrete magnitudes $A_k$ are calculated from the PSD of the phase noise $L(f)$ as follows,

$$A_k = \sqrt{P_r\, L(f_k)}, \quad (12)$$

where $P_r$ is the power of the received signal. The Discrete Inverse Fourier Transform (DIFT) is then applied to get the time samples of the noisy received signal,

$$s(t) = \text{DIFT}(S_k). \quad (13)$$

The corresponding instantaneous phase error, $\varphi_e(t)$ can be calculated as,

$$\varphi_e(t) = \tan^{-1}\left(\frac{\text{imag}(s(t))}{\text{real}(s(t))}\right) - (2\pi f_c t + \psi_{m,n}). \quad (14)$$

## V. ADDITIVE GAUSSIAN NOISE MODEL

The additive noise samples in this study are modeled as a normal distributed random samples with zero-mean and standard deviation $\sigma$, its probability density function (pdf) has the form:

$$G(n) = \frac{1}{\sigma\sqrt{2\pi}} e^{-n^2/2\sigma^2}, \quad (15)$$

where n is the random variable that represents the instantaneous values corresponding to the white Gaussian noise. In the frequency domain $\mathbf{N}(\theta_p)$ can be obtained by applying the fast Fourier transform on the time samples $i = 1, 2, 3, \ldots \text{I}$:

$$N(\theta_p) = \text{FFT}(n(\theta_p)). \quad (16)$$

## VI. RESULTS AND DISCUSSIONS

### A. Performance assessment of the proposed Yagi-Uda antenna

The Rogers RO3003C™ with dielectric constant $\varepsilon_r = 3$, dielectric loss tangent $\tan\delta = 0.0021$, and height $h = 0.25$ mm is used for the design of the proposed Yagi-Uda antenna. The metal parts of the antenna are made of copper with conductivity $\sigma = 5.6 \times 10^7 \text{S/m}$ and thickness t = 0.032 mm. The design parameters are listed in Table 1. The antenna is placed in the $xy$-plane with the feed line aligned with the $x$-axis. The dependency of the reflection coefficient, $|S_{11}|$, on the frequency over a wide band is presented in Fig. 3. It is clear that the impedance is perfectly matched at the two frequencies 28 and 38 GHz with reflection coefficients $-27$ and $-26$ dB, respectively. At 28 GHz, the band width is about 3.32 GHz, whereas at 38 GHz, the band width is about 1.4 GHz. The radiation efficiencies are 96.3% at 28 GHz and 95.2% at 38 GHz.

The normalized radiation patterns for the proposed dual-band Yagi-Uda antenna at 28 GHz and 38 GHz in the planes $\phi = 0^\circ (xz-plane)$ and $\theta = 90^\circ (xy-plane)$ are presented in Figs. 4 (a) and 4 (b), respectively. The maximum gain is 9.3 dBi at 28 GHz with SLL -11 dB and 9.8 dBi at 38 GHz with SLL -10.1 dB.

Table 1: dimensional parameters for the proposed Yagi-Uda antenna

| Name | Value (mm) | Name | Value (mm) |
|---|---|---|---|
| $L_a$ | 2.4 | $W_{t1}$ | 0.5 |
| $L_{t1}$ | 3.62 | $L_{t2}$ | 4.02 |
| $W_{r2}$ | 1.0 | $D_r$ | 1.95 |
| $L_{r2}$ | 3.4 | $L_d$ | 2.79 |
| $W_{t2}$ | 0.62 | $W_{t3}$ | 0.35 |
| $L_{t3}$ | 2.5 | $W_{r1}$ | 1.0 |
| $W_G$ | 6.72 | $L_{r1}$ | 7.6 |
| $L_e$ | 0.8 | $W_e$ | 0.2 |

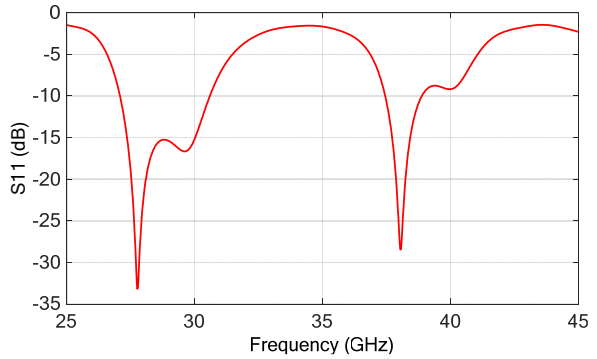


Fig. 3. The frequency response of the reflection coefficients $|S_{11}|$ of the proposed Yagi-Uda antenna with the dimensional parameters listed in Table 1.

**B. Performance assessment of the Yagi-Uda array**

An eight-element linear array of the proposed Yagi-Uda antenna is constructed and arranged on the $y-$ axis. For good beam-steering and in order to reduce the side lobes the distance between the array elements is set to $D_y = 8.85\,mm$ as shown in Fig. 5. This means that the elements are overlapped as shown in the figure with each two adjacent antennas sharing a common reflector. The total array dimensions are $79.4\text{ mm} \times 9.65\text{ mm}$ excluding the feeding microstrip line. The frequency response of the reflection coefficient and the coupling coefficients for the array elements are shown in Fig. 6 and Fig. 7, respectively. Also the radiation patterns for the proposed linear array at the operating frequencies 28 and 38 GHz are shown in Fig. 8.

**C. Evaluation of the steering matrix of the proposed array**

Instead of using the simple and approximate expressions (1-3) to evaluate the steering matrix for the proposed linear array of Yagi-Uda elements, it can be evaluated more accurately by rigorous numerical techniques. The commercial available CST® package is used for this purpose by calculating the received voltage signals at each of the array elements due to a plane wave incident on the array in the plane $\phi = 90^\circ$ and making an angle $\theta$ with the $z-$ axis. With varying the angle $\theta$, the steering matrix of this linear array can be accurately evaluated. In this way the steeing matrix in (4) can be evaluated. The relation between the direction, $\theta$, of the main beam and the progressive phase shift, $\beta$, is obtained by feeding the array elements with the progressive phase shifts ranging from $0°$ to $180°$ and then calculating the corresponding direction, $\theta$, of the main beam through electromagnetic simulation. The relationship between $\beta$ and $\theta$ is plotted in Fig. 9 (a). As shown in Fig. 9 (b), the gain of the Yagi-Uda array decrease as the steering angle of the radiation pattern is increased moving away from the direction normal to the array. The radiation patterns at different steering angles are shown in Fig. 10 (a) and Fig. 10 (b) at 28 and 38 GHz, respectively.

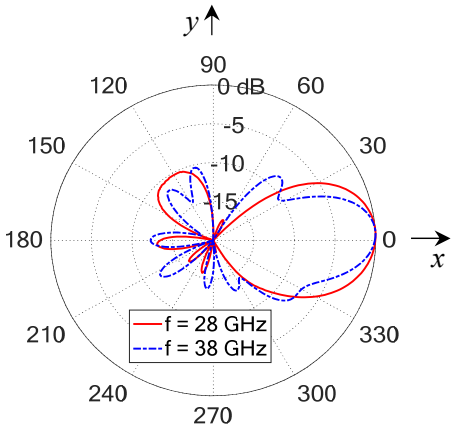


(a) $\theta = 90^\circ\ (xy-plane)$

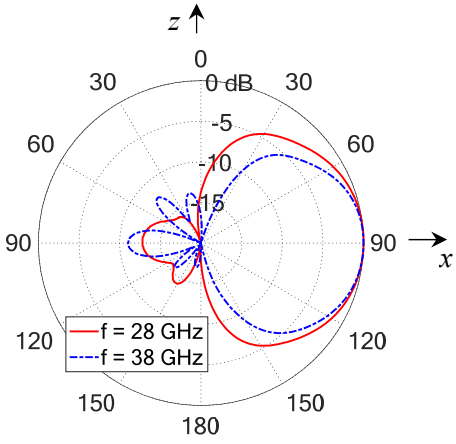


(b) $\phi = 0^\circ (xz-plane)$

Fig. 4. Normalized radiation patterns of the proposed dual-band antenna at 28 and 38 GHz in the $xy-plane$ ($\theta = 90^\circ$) and $xz-plane$ ($\phi = 0^\circ$).

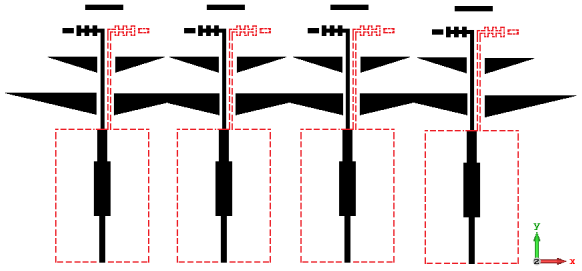

Fig. 5. Part of the eight overlapped elements linear array of the proposed Yagi-Uda antenna.

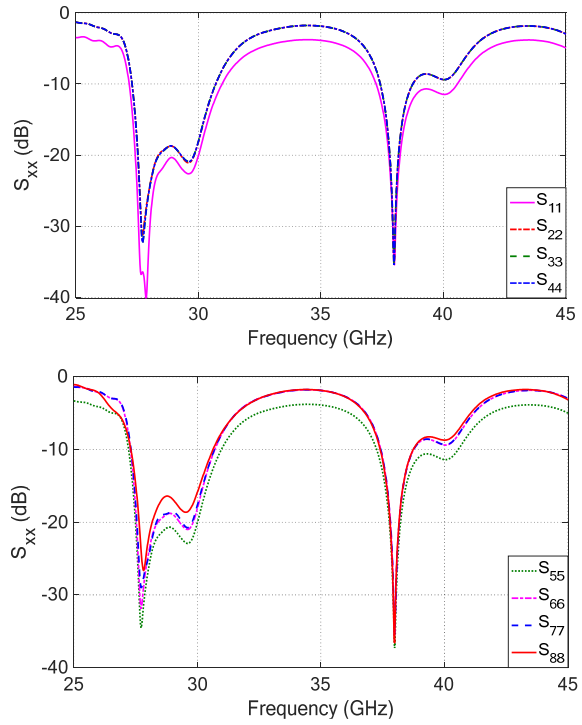


Fig. 6. The frequency response of the reflection coefficients $|S_{nn}|$ of each element of the proposed Yagi-Uda antenna array.

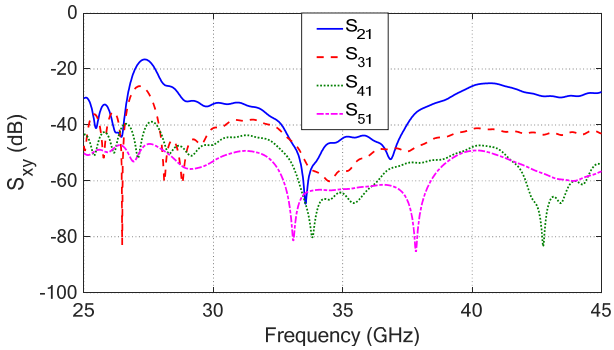


Fig. 7. Coupling coefficients of the proposed linear array of Yagi-Uda elements.

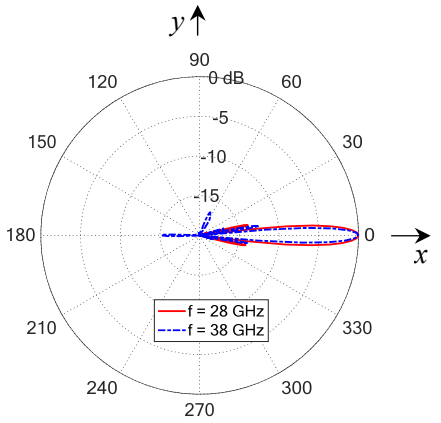


(a) $\theta = 90^{\circ}$ $(xy - plane)$

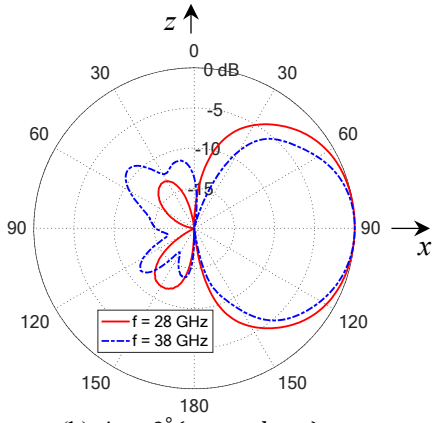


(b) $\phi = 0^{\circ}(xz - plane)$

Fig. 8. Normalized radiation patterns of the proposed linear array at 28 and 38 GHz in the $xy - plane$ ($\theta = 90^{\circ}$) and $xz - plane$ ($\phi = 0^{\circ}$).

**D. DoA estimation of multiple signals using PCMA algorithm in the absence of noise**

Three plane wave sources are assumed incident on the proposed Yagi-Uda linear array producing electromagnetic waves impinging on the antenna array from the directions $\theta = 10^{\circ}, 20^{\circ}$, and $40^{\circ}$. The electromagnetic simulation is performed to calculate the received voltage signals at each of the antenna array elements to get the matrix described by (4). No noise is added to the received signals. The received data due to the three signals coming simultaneously from the directions indicated are calculated through computer simulation using CST®. The normalized $P_{CMA}(\theta)$ function given by (8) is calculated using the steering matrix calculated as described in Section 4 and is plotted against $\theta$ as shown in Fig. 11 for $SNR \approx \infty$. The normalized $P_{CMA}(\theta)$ function shown in Fig. 11 has three peaks whose directions are assumed to give the three directions of arrival. Due to the high level of the SNR, it is found that the peaks of the normalized correlation function lie exactly at $\theta = 10^{\circ}, 20^{\circ}$, and $40^{\circ}$, that is, the

directions of arrival are retrieved exactly without any error.

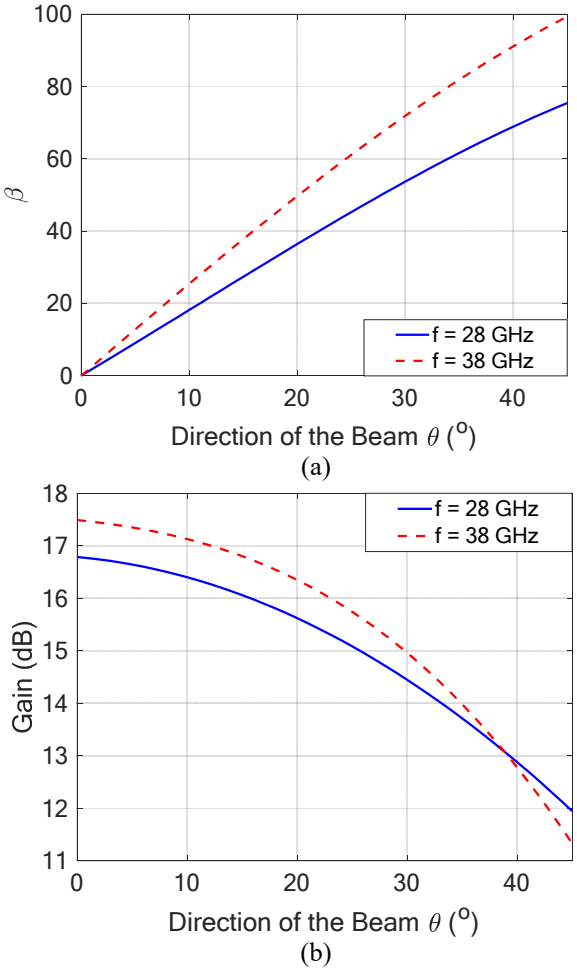


Fig. 9. The change in the (a) progressive phase shift $\beta$, and (b) maximum gain with the direction, $\theta$, of the steered beam.

### E. Effect of noise on the DoA estimation

For realistic simulation of the signals received at the array elements, phase noise and additive Gaussian noise are generated and added to the received signals (after being calculated by the CST®) as described in Sections 4 and 5 to get actual received signals.

### E.1. Effect of phase noise

The effect of phase noise on the error in the estimation of DoA is investigated under the assumption that the received signals are affected by phase noise with PSD as that presented in Fig. 12 (a). The instantaneous phase noise samples $\varphi_e(t)$ are calculated as expressed in equation (14) and plotted in Fig. 12 (b) and also the NCR is obtained as given by (9b). The Error in DoA estimation by increasing the NCR is investigated for the directions $\theta = 10^\circ, 20^\circ, 30^\circ$, and $40^\circ$. The resulting error in the estimated DoA are plotted against NCR in Fig. 13. For realistic simulation the phase error samples are, first, calculated and, then, added to the samples of the received signals at the array elements which have been already calculated using the CST®. The PCMA algorithm is, then, applied to estimate the DoA.

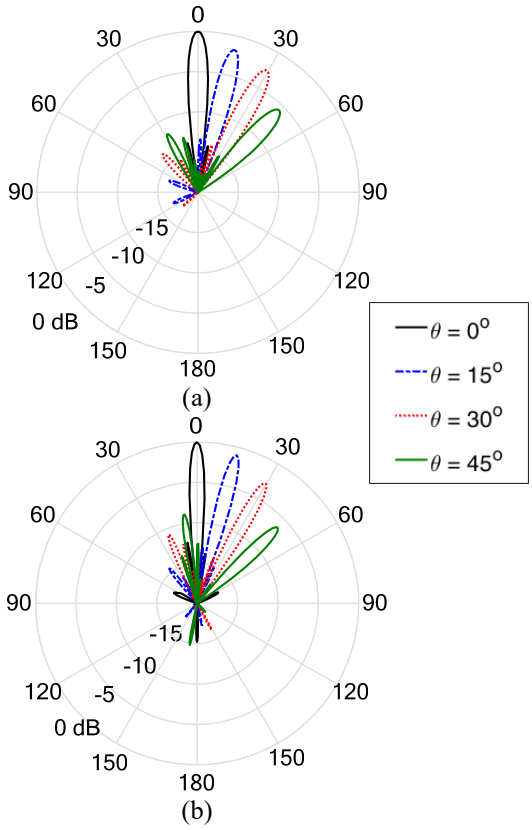


Fig. 10. The steered beam at different directions using the proposed linear array at: (a) 28 GHz and (b) 38 GHz.

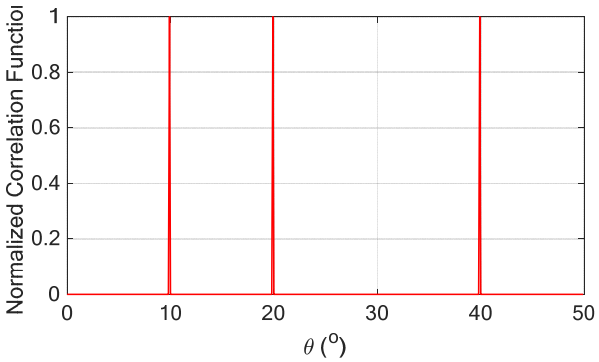


Fig. 11. Normalized correlation function in case of three received signals coming from the directions $\theta = 10^\circ$, $20^\circ$, and $30^\circ$ under the assumption of very high SNR for each signal.

It is shown in Fig. 13 that the error in the estimated DoA increases with increasing the NCR. Also, it is shown that the error increases with increasing $\theta$, i.e., the error in the estimated DoA increases as the received signal is incoming from a direction father away from the normal to the linear array.

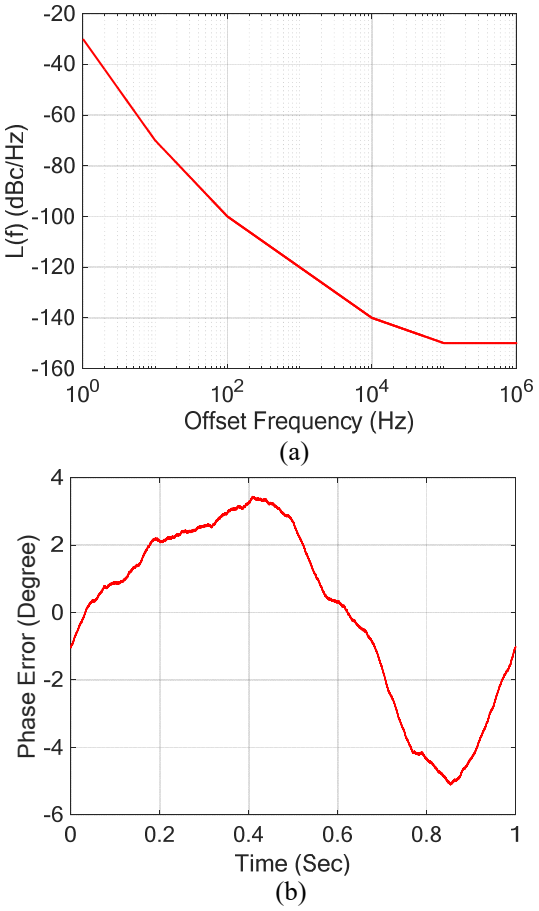


Fig. 12. Phase Noise characteristics: (a) $L(f)$ and (b) corresponding phase error time samples.

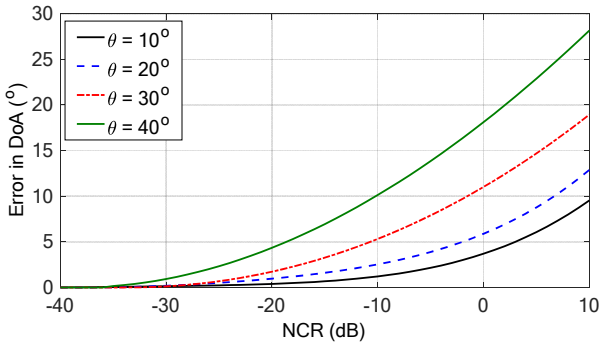


Fig. 13. Error in DoA estimation by increasing the noise to carrier power ratio (NCR) for different angles of reception.

**E.2. Effect of additive noise**

In this section, the method described for DoA estimation using the proposed Yagi-Uda array is examined in the presence of additive white Gaussian noise. The noise samples are generated and added to the received voltages at the different array elements as explained in Section 5.2, then the DoA is calculated. The angle of arrival of the received signal at different values of the SNR is estimated using the PCMA algorithm and plotted in Fig. 14. It is shown that the error in the estimated value of the DoA decreases with increasing the SNR. It is noticeable that as the signal is coming from a direction father from the normal to the array, the error in the estimated DoA increases.

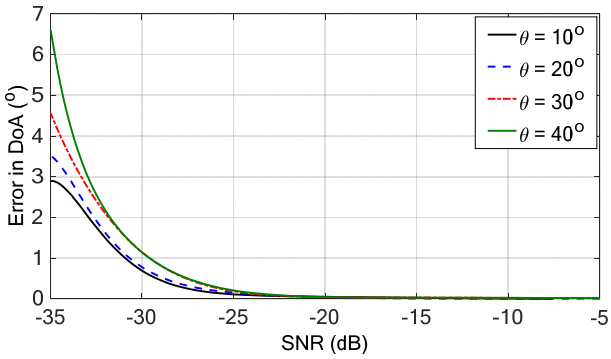


Fig. 14. Effect of additive white Gaussian noise on the error in DoA estimation for different direction of the incoming signal.

**E.3. Receiving multiple signals in the presence of noise**

In this section, the efficiency of the proposed linear array to estimate the DoA of multiple signals under the effect of phase noise and additive noise using the PCMA technique is numerically investigated. The CST® simulator is used to obtain the steering matrix for the array in the range $0^{\circ} < \theta < 45^{\circ}$ such that the side lobe level $\leq -13$ dB, and the gain $\geq 15$ dB. The steering matrix for the array is saved and stored for post processing. Four plane waves are simultaneously incident on the antenna array from different directions as listed in Table 2. For realistic simulation, the incoming signals are affected by different values of the phase and additive noise power. Thus, the estimated angles of arrival of the incoming waves are obtained for different values of the NCR and SNR as listed in Table 2. Figure 15 shows the normalized correlation function given by (8) for four incoming signals, each has a different noise to carrier power ratio.

**F. Fabrication and measurements**

This section is concerned with the experimental investigation of the characteristics of the proposed Yagi-

Uda antenna and the performance of the proposed MIMO array. For this purpose a prototype is fabricated for the Yagi-Uda antenna and another prototype is fabricated for four-element linear array.

Table 2: The estimated DoA for four plane waves coming from different directions affected by phase and additive noise of different power levels

| Incoming DoA | Phase Noise NCR (dB) | Additive Noise SNR (dB) | Estimated DoA | Error (%) |
|---|---|---|---|---|
| $\theta = 10^{\circ}$ | -25 | -5 | 10 | 0 |
| $\theta = 20^{\circ}$ | -30 | -10 | 20 | 0 |
| $\theta = 30^{\circ}$ | -8 | -20 | 31.6 | 5.3 |
| $\theta = 40^{\circ}$ | -15 | -10 | 39.8 | 0.5 |

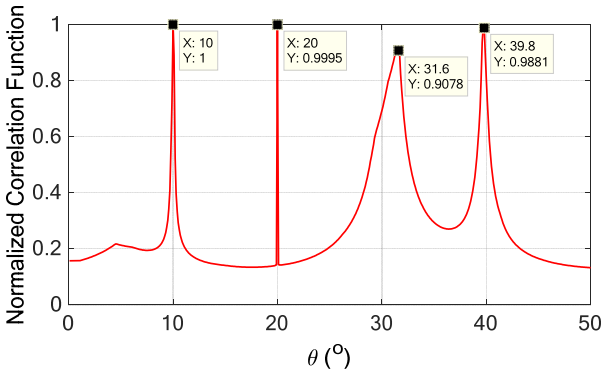


Fig. 15. Normalized PCAMA of four incoming signals on the proposed linear array of Yagi-Uda elements.

### F.1. Single element Yagi-Uda antenna

For experimental verification, a prototype for the Yagi-Uda antenna is fabricated and it performance is evaluated through experimental measurements. The dependence of the reflection coefficient on the frequency is measured in the frequency band 25-45 GHz. Rogers RO3003™ with dielectric constant $\varepsilon_r = 3$, loss tangent $\delta = 0.0013$, and height $h = 0.25$ mm, is the substrate used for fabrication. The design dimensions for the single-element Yagi-Uda antenna are listed in Table 1. Figure 16 shows the photos of the fabricated prototype connected to a 2.4 mm coaxial end launch connector from the top and bottom views. The frequency dependence of the reflection coefficient $|S_{11}|$ of the antenna input port is measured using the vector network analyzer (VNA) Rohde and Schwartz model ZVA67 and plotted in Fig. 17 (a). Figure 17 (b) shows the fabricated antenna connected to the VNA ZVA67 for measuring the return loss. The measured frequency response of $|S_{11}|$ is compared with the simulation results obtained using the CST® simulator in the same figure. Good agreement is shown between the simulation and the measured return loss. The impedance matching bandwidth for a return loss $\leq -10$ dB is about 2.6 GHz at 28 GHz and 1.35 GHz at 38 GHz.

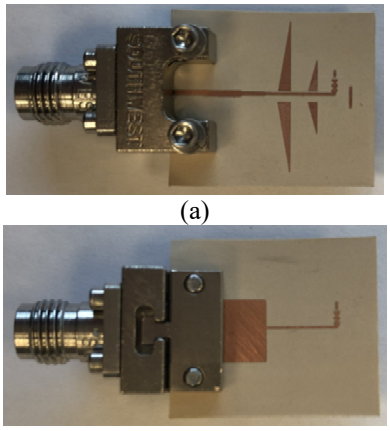

(a)

(b)

Fig. 16. (a) Top and (b) bottom views of the fabricated prototype Yagi-Uda dual-band (28/38 GHz) antenna connected to a 2.4 mm end-launch coaxial connector.

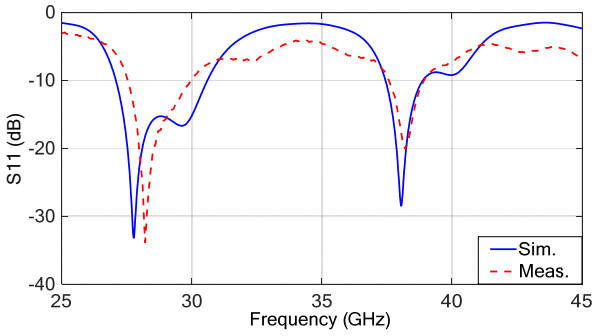


(a)

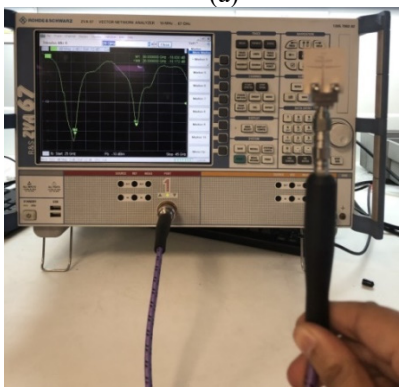

(b)

Fig. 17. (a) Measured return loss of the dual-band antenna with frequency compared with the simulation results. (b) The proposed dual-band Yagi-Uda antenna connected to the ZVA67 VNA.

The radiation patterns of the fabricated Yagi-Uda antenna are measured at 28 and 38 GHz using a standard gain horn antenna model LB-018400 in the principal planes $x-y$ ($\theta = 90°$) and $x-z$ ($\phi = 0°$). The antenna under-test (proposed Yagi-Uda) and the LB-018400 are placed in an anechoic chamber at a distance of 60 cm. The experimental setups for measuring the radiation patterns of the proposed antenna using the VNA of the Rohde and Schwartz ZVA67 are shown in Fig. 18. The reference standard gain horn antenna model LB-018400 is connected to port '2' of the VNA whereas the antenna under test is connected to port '1' to obtain its radiation pattern by measuring the transmission coefficient $|S_{21}|$ at the frequencies of concern. The two-dimensional radiation patterns at 28 and 38 GHz obtained by measurements are presented in Fig. 19 and Fig. 20, respectively, in the $xy$ and $xz$ planes, in comparison to that obtained by simulation showing good agreement.

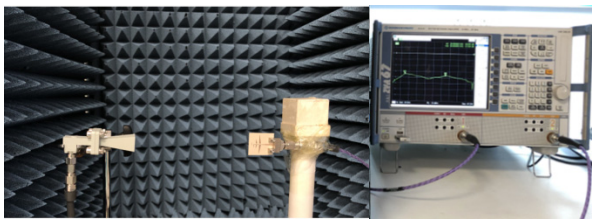

Fig. 18. Experimental setup for measuring the radiation pattern of the proposed dual-band Yagi-Uda antenna.

**F.2. Four-element linear array of the proposed Yagi-Uda antenna**

A four-element array of the printed Yagi-Uda antenna is fabricated to assess the array performance and compare the measurements with the electromagnetic simulations results. Due to the limiting dimensions of the end-launch connector size, the fabricated array has four elements separated by interelement spacing $D_y$ 18 mm. The fabricated array is shown in Fig. 21. The simulated and measured dependency of the reflection coefficient $|S_{nn}|$ of each element on frequency is plotted in Fig. 22 (a) and 22 (b), respectively. In Fig. 23 (a) and 23 (b), the simulated and measured coupling coefficient $|S_{mn}|$ between the array elements is measured versus the frequency. It is clear from Fig. 22 that the fabricated array is matched at both of the operating frequencies 28 and 38 GHz. Also, it is shown in Fig. 23 that the MIMO array has very low coupling coefficients which make it suitable for MIMO systems that use multiple antennas to create different transmission paths for spatial diversity. The frequency responses of the envelope correlation coefficient (ECC) and the diversity gain (DG) of the proposed four-element array MIMO system are presented in Fig. 24. It is shown that the ECC is almost 0 and, consequently, the DG is almost 10 over the lower and upper frequency bands (centered at 28 and 38 GHz, which is the best achievable performance for a MIMO antenna system. The radiation patterns of the fabricated array are measured and compared to the radiation patterns obtained by electromagnetic simulation in the two planes $x-y$ ($\theta = 90°$) and $x-z$ ($\phi = 0°$) and presented in Figs. 25 and 26, respectively, showing excellent agreement.

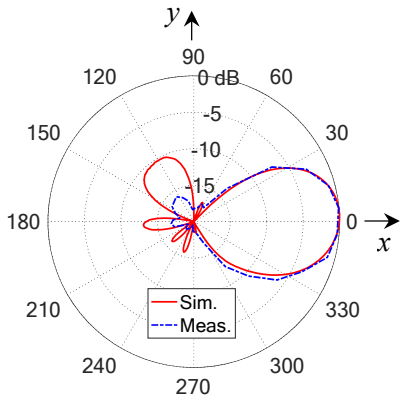


(a) $f = 28$ GHz, $\theta = 90°(xy-plane)$

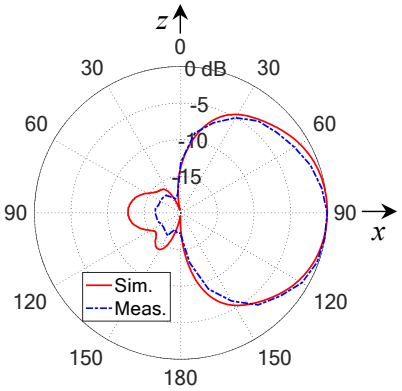


(b) $f = 28$ GHz, $\phi = 0°(xz-plane)$

Fig. 19. Measured radiation patterns of the dual-band Yagi-Uda antenna compared with the simulation results at 28 GHz.

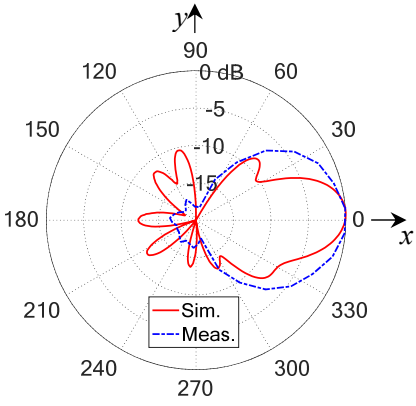


(a) $f = 38$ GHz, $\theta = 90°(xy-plane)$

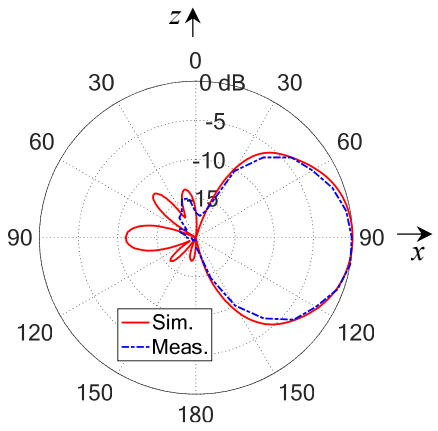


(b) $f = 38$ GHz, $\phi = 0°(xz-plane)$

Fig. 20. Measured radiation patterns of the dual-band Yagi-Uda antenna compared with the simulation results at 38 GHz.

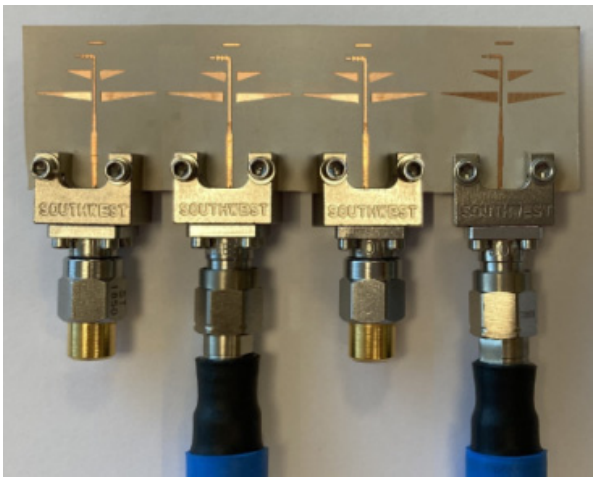

Fig. 21. Fabricated linear array composed of four elements of the proposed Yagi-Uda antenna.

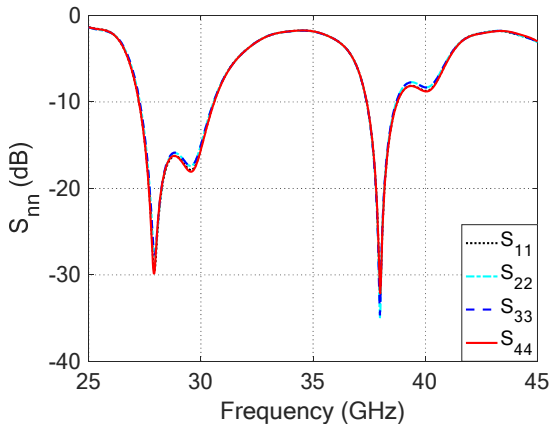


(a)

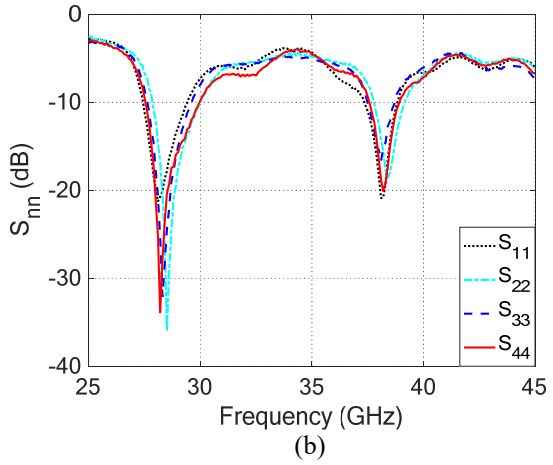


(b)

Fig. 22. (a) Simulated and (b) measured, reflection coefficients of the four elements of the fabricated array shown in Fig. 20.

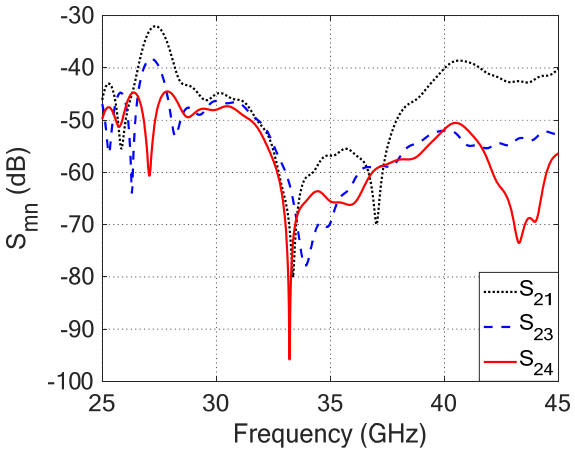


(a)

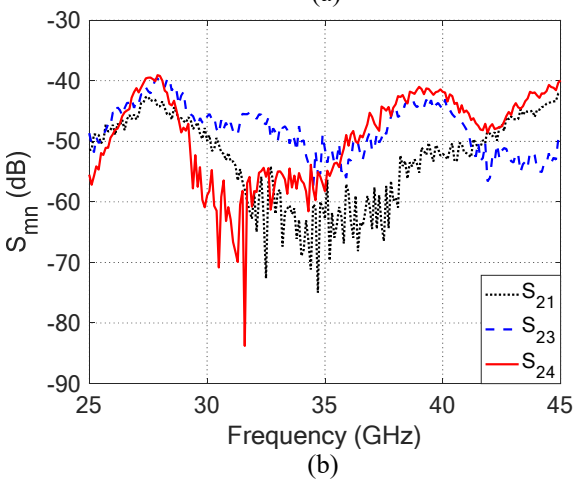


(b)

Fig. 23. (a) Simulated and (b) measured coupling coefficients between the elements of the fabricated array shown in Fig. 21.

A comparison between the proposed design and the antennas proposed in literature for mm-wave applications is performed. The proposed Yagi-Uda is compared to similar Yagi-Uda antennas in literature. The comparison criteria are the size, number of bands, the bandwidth for each band, and antenna gain, which are presented in Table 3. To the best of our knowledge, the present work proposes a dual-band Yagi-Uda antenna for MIMO applications which is not found in literature. In addition to its dual-band operation, the proposed design still has compact size, high gain, bandwidth, very low mutual coupling, and very high radiation efficiency, and it also has nearly perfect ECC and DG.

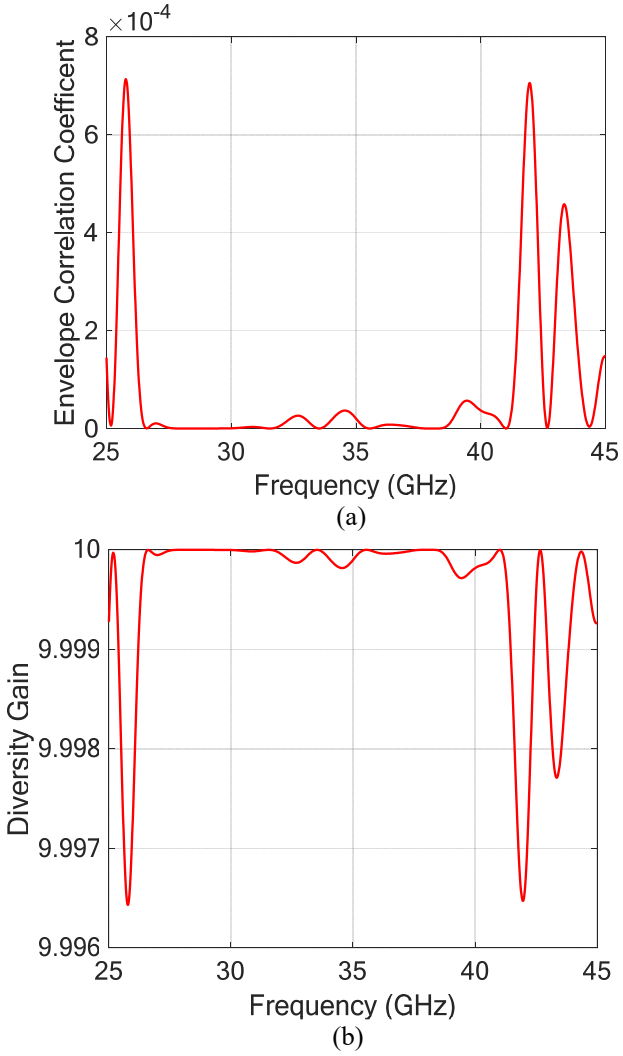


Fig. 24. Frequency dependence of the ECC and DG of the 4-port MIMO antenna proposed in the present work.

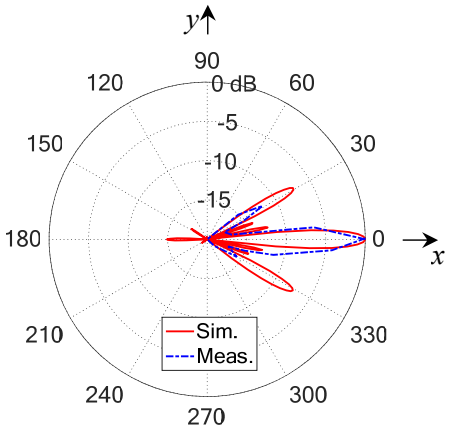


(a) $f = 28$ GHz, $\theta = 90°(xy-plane)$

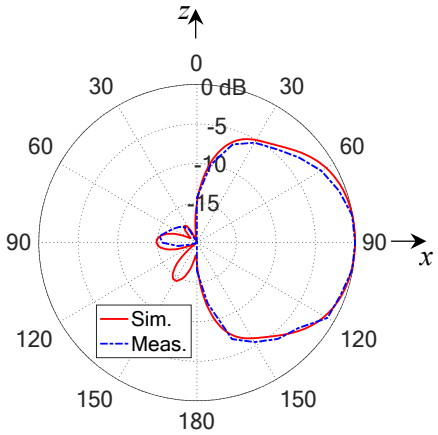


(b) $f = 28$ GHz, $\phi = 0°(xz-plane)$

Fig. 25. Measured radiation patterns of the fabricated four elements linear array compared with the simulation results at 28 GHz.

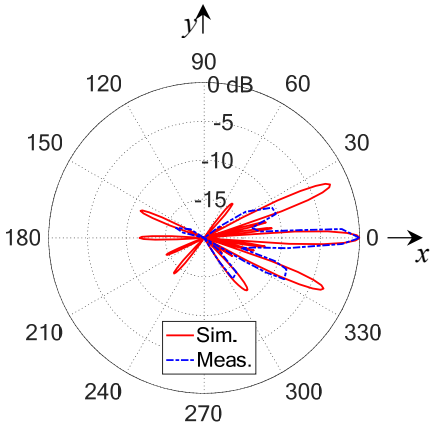


(a) $f = 38$ GHz, $\theta = 90°(xy-plane)$

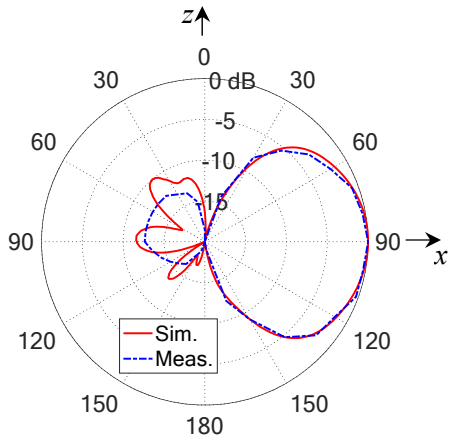


(b) $f = 38$ GHz, $\phi = 0°(xz-plane)$

Fig. 26. Measured radiation patterns of the fabricated four elements linear array compared with the simulation results at 38 GHz.

Table 3: Comparison with similar Yagi-Uda antennas for MIMO in literature

| | [17] | [18] | [19] | Present Work |
|---|---|---|---|---|
| Size | 14.8x5.1 | 11.2x8.1 | 40.7x22.9 | 9.7x18.2 |
| Substrate Height (mm) | 0.2 | 0.25 | 0.38 | 0.25 |
| Number of bands | 1 | 1 | 1 | 2 |
| Freq. of first band (GHz) | 28 | 24 | 24 | 28 |
| Freq. of second band (GHz) | --- | --- | --- | 38 |
| BW of first band | 3.7 | 0.7 | 4.1 | 3.42 |
| BW of second band | --- | --- | --- | 1.45 |
| Gain (dBi) | 8 | 9.3 | 8 | 9 |

## VII. CONCLUSIONS

In this paper a dual-band (28/38 GHz) linear antenna array is proposed to work as a MIMO array for the 5G communication systems. Each element in the array is a dual-band Yagi-Uda antenna that is well designed at the 28 and 38 GHz. The array is composed of eight elements with total dimension of 79.4 mm × 9.65 mm excluding the feeding microstrip line. The array exhibits a high gain about 18 dB in the forward direction. The PCAMA direction of arrival estimation technique is applied to the received signals at the array elements to determine the direction of arrival for multiple incoming signals. The effect of phase noise and additive Gaussian noise on the error in the DoA estimation are studied showing good accuracy of the PCAMA algorithm. Numerical and experimental investigations are achieved to assess the performance of both the single-element antenna and the eight element MIMO linear antenna array. It is shown that the simulation results agree with the experimental measurements and both show good performance of the single antenna as well as the MIMO linear array system. The radiation pattern for single element and four element array are measured and compared to the electromagnetic simulation results showing good agreement.

## REFERENCES

[1] T. S. Rappaport, S. Sun, R. Mayzus, H. Zhao, Y. Azar, K. Wang, G. N. Wong, J. K. Schulz, M. Samimi, and F. Gutierrez, "Millimeter wave mobile communications for 5G cellular: It will work!," *IEEE Access*, vol. 1, pp. 335-349, 2013.

[2] T. S. Rappaport, F. Gutierrez, E. Ben-Dor, J. N. Murdock, Y. Qiao, and J. I. Tamir, "Broadband millimeter-wave propagation measurements and models using adaptive-beam antennas for outdoor urban cellular communications," *IEEE Trans. Antennas Propag.*, vol. 61, no. 4, pp. 1850-1859, 2013.

[3] C. Narayan, *Antennas and Propagation*. Technical Publications, 2007.

[4] A. V. Alejos, M. G. Sanchez, and I. Cuinas, "Measurement and analysis of propagation mechanisms at 40 GHz: Viability of site shielding forced by obstacles," *IEEE Trans. Veh. Technology*, vol. 57, no. 6, pp. 3369-3380, 2008.

[5] S. Rajagopal, S. Abu-Surra, Z. Pi, and F. Khan, "Antenna array design for multi-gbps mm wave mobile broadband communication," in *Global Telecommunications Conference (GLOBECOM). IEEE*, pp. 1-6, 2011.

[6] A. I. Sulyman, A. T. Nassar, M. K. Samimi, G. R. MacCartney, T. S. Rappaport, and A. Alsanie, "Radio propagation path loss models for 5G cellular networks in the 28 GHz and 38 GHz millimeter wave bands," *IEEE Communications Magazine*, vol. 52, pp. 78-86, 2014.

[7] M. S. Sharawi, S. K. Podilchak, M. T. Hussain, and Y. M. M. Antar, "Dielectric resonator based MIMO antenna system enabling millimeter-wave mobile devices," *IET Microwaves, Antennas & Propagation*, pp. 287-293, 2017.

[8] D. T. T. Tu, N. G. Thang, and N. T. Ngoc, "28/38 GHz dual-band MIMO antenna with low mutual coupling using novel round patch EBG cell for 5G applications," *International Conference on Advanced Technologies for Communications*, 2017.

[9] J.-F. Li and Q.-X. Chu, "A compact dual-band MIMO antenna of mobile phone," *Journal of Electromagnetic Waves and Applications*, vol. 25, pp. 1577-1586, 2011.

[10] M. I. Khattak, A. Sohail, U. Khan, Z. Barki, and G. Witjaksono, "Elliptical slot circular patch antenna array with dual band behavior for future 5G mobile

communication networks," *Progress in Electromagnetics Research C*, vol. 89, pp. 133-147, 2019.

[11] M. V. Madhava, N. S. Jagadeesha, and T. Yerriswamy, "A comparative study of DoA estimation algorithms with application to traking using Kalman filter," *Signal & Image Processing: An International Journal (SIPIJ)*, vol. 6, no. 6, Dec. 2015.

[12] M. Li, Y. Lu, and B. He, "Array signal processing for maximum likelihood direction-of-arrival estimation," *Journal of Electrical & Electronic Systems*, 2013.

[13] M. Devendra and K. Manjunathachari, "DOA estimation of a system using MUSIC method," *International Conference on Signal Processing and Communication Engineering Systems*, 2015.

[14] R. Roy, A. Paulraj, and T. Kailath, "ESPIRT-estimation of signal parameters via rotational invariance techniques," *IEEE Trans. Acoust. Speech Signal Process*., vol. 34, no. 5, pp. 1340-1342, 1989.

[15] A. E. Farahat and K. F. A. Hussein, "Effect of phase noise on two-angle DoA estimation using planar arrays," *The 4th International Conference on Advanced Technology & Applied Sciences (ICaTAS2019)*, 2019.

[16] A. E. Farahat and K. F. A. Hussein, "Efficient computational model of phase noise and its applicability to assess the performance of digital modulation techniques," *Applied Computational Electromagnetics Society Journal*, vol. 34, no. 12, pp. 1931-1941, 2019.

[17] M. R. Naeini and M. Fakharzadeh, "A 28 GHz beam-switching Yagi-Uda array using Rotman lens for 5G wireless communications," *International Symposium on Antennas and Propagation & USNC/URSI National Radio Science*, 2017.

[18] P. R. Grajek, B. Schoenlinner, and G. M. Rebeiz, "A 24-GHz high-gain Yagi-Uda antenna array," *IEEE Trans. Antennas Propag*., vol. 52, pp. 1257-1261, May 2004.

[19] R. A. Alhalabi and G. M. Rebeiz, "High-gain Yagi-Uda antennas for millimeter-wave switched beam systems," *IEEE Trans. Antennas Propag*., vol. 57, no. 11, pp. 3672-3676, Nov. 2009.